NRIAG JOURNAL OF ASTRONOMY AND GEOPHYSICS
2020, VOL. 9, NO. 1, 280–288
https://doi.org/10.1080/20909977.2020.1746894

Application of magnetic and resistivity for groundwater investigations at North Al Ain Sokhona – Cairo Road, Al Ain Sokhna, Egypt

Sultan Awad Sultan Araffa[a], Hassan Saleh Sabet[b] and Mahmoud Ahmed Abed[b]

[a]Geomagnetic and Geoelectric Department, National Research Institute of Astronomy and Geophysics, Helwan, Egypt; [b]Geology Department, Faculty of Science, Al Azhar University, Cairo, Egypt

ABSTRACT

The present study aims to delineate different types of the ground water accumulations in the northwest Gulf of Suez using geoelectrical and magnetic measurements. Twenty-one Vertical Electrical Soundings (VES) to determined groundwater potentialities. Based onthe quantitative geoelectrical analysis, the subsurface sequence consists of six geoelectrical layers; The first layer belonging to Quaternary period and built up of dry sand and gravels. The second layer belonging to the upper Miocene and built up of sandstone and limestone. The thirdlayer belonging to middle Miocene and formed of limestone and sandy clay. The fourth layer belonging to lower Miocene and composed of limestone and clayey limestone. The fifth layer belonging to the Oligocene and Upper Eocene clay and consists of clayey and sandstone. The sixth layer belonging to the Middle Eocene composed of limestone. Quantitative geoelectrical analysis of the study area also concluded that there are two water-bearing geoelectrical layers (aquifers), the second geoelectric unit represents the fresh water aquiferwhile the third geoelectric unit layer represents the brackish aquifer. The results of magnetic interpretation indicate that the area under study dissected by fault elements of N-S and NE-SW. The depth to the basement ranges from (1925–1998 m).

ARTICLE HISTORY
Received 24 January 2020
Revised 12 February 2020
Accepted 26 February 2020

KEYWORDS
Geoelectric; groundwater; fault; magnetic and basement

1. Introduction

The study area has a surface area of about 20 Km^2 between latitudes 29° 43′ 30″ N and 29° 45′ 25″ N and Longitudes 32° 18′ 25″ E and 32° 14′ 50″ E lies at northwest Gulf of Suez. The area under study represents an important centre for tourist, mining activities, and industrial projects. It lies at distance 3700 m from the Cairo-Al Ain Sokhna road and distance 5000 m from Suez-Al Ain Sokhna road (Figure 1(a)). Many authors have carried out valuable geological, structural, geophysical and hydrological works around the Focus area as Sadek (1926); Ghorab (1961); Abdallah et al. (1963); Awad and Abdallah (1966); Desouki et al. (2006); Hassan (2008), Farhoud (2009); El Osta et al. (2010); Araffa et al. (2014); Hewaidy et al. (2015); Araffa et al. (2017); Sultan et al. (2017); Abdellatif et al. (2019).

2. Geology of the study area

In the study area, different rock units were identified. They range in age from the Jurassic to Quaternary (Figure 1(b)). Marine Jurassic sediments are exposed in the foothills of El Galala El Bahariya Plateau. Bathonian strata is composed of limestones, marls, and sandstones. Middle Callovian, Oxfordian, and Kimmeridgian sandstones, shales, and limestones up to 30 m thick have been described from Abu Darag and Wadi Qiseib Abdallah et al (19633, El Shazly (1977). The lower Cretaceous Malha Formation named by Abdallah et al. (1963) exposed on the southeast flanks of El Galala El Bahariya Plateau, continental to shallow marine, snow white, violet, and pinkish sandstone with clay intercalations and kaolin deposits, including marine interbeds Abdallah et al (19633, El Shazly (1977) Ghorab (1961) assigned nomenclature for the Upper Cretaceous rocks in the Gulf of Suez region from base to top as:Raha (Cenomanian age equivalent to Galala Formation, Awad and Abdallah (1966), Wata (Turonian age), Matulla (Early Senonian age) and Sudr (Late Senonian age) formations, Ball (1900) named the green to grey shale Palaeocene by Esna shale. The lower Eocene section outcrops are composed of three main parts of total thickness measures about 200 m. The lower part consists of light yellow fine-grained foraminiferal limestone rich, while the other two parts are composed of very fine-grained Nummulitic limestone Abdel Khalek (2014). Middle Eocene differentiated into Muweilih, Mokattam, Observatory, Qurn and Wadi Garawi formations Farag and Ismail (1959), Said (1962), Strougo (1986). Upper Eocene rocks are made up of brown sandy limestones, marls, and shales with some sandstone interbeds Hassan (2008). The Oligocene sedimentary section can be classified into two units: The lower unit consists of varicoloured, poorly lithified sands and

CONTACT Sultan Awad Sultan Araffa sultan_awad@yahoo.com National Research Institute of Astronomy and Geophysics, Helwan, Egypt

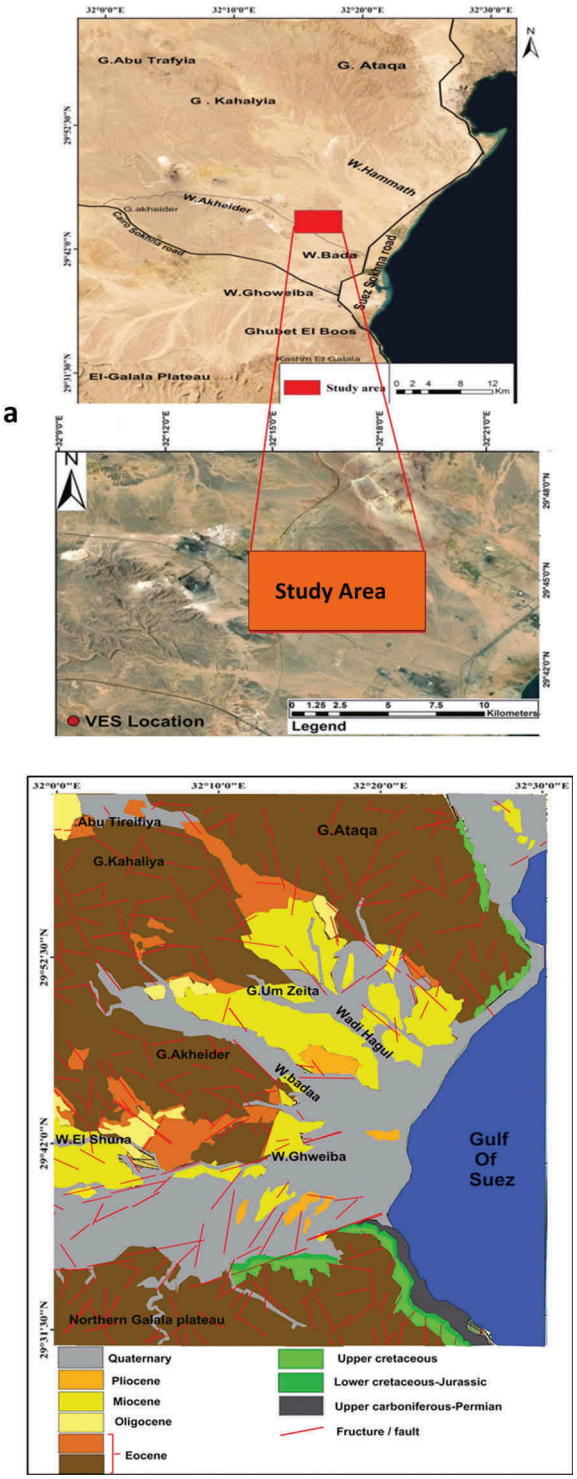

Figure 1. (a) Location map of the study area, (b) Geological and structure map of the study area (modified after Conoco 1987).

gravels and change to cross bedded hard sandstone with highly silicified conglomeratic beds. The upper unit of white and yellow sand beds. The whole sequence is capped with sheet of Oligo-Miocene Sadek (1926) vesicular and amygdaloidal basaltic flow Abdel Khalek (2014). The Miocene sediments differentiated into: Marine Miocene unit marls, calcareous sandstones and Non-Marine Miocene dark yellow sandstones, gravels and chalky sandstones. The Pliocene section consists of limestone, clays and poorly lithified sands and gravels while the Quaternary rocks consist of unlithified alluvial sediments Abdel Khalek (2014).

3. Methodology

3.1. Measurements and interpretation of magnetic data

3.1.1. Measurements and enhancement of magnetic data

The measurements are carried out on the stations every 200 m by the Geologic Survey of Egypt using two magnetometers model Envi-Mag made by Scintrex company, Canada. One instrument used for field survey and second instrument used for base station to apply diurnal variation. Also, IGRF correction is applied, the corrected magnetic data are used to construct total intensity magnetic map. The total intensity magnetic map (Figure 2(a)) can be described as the total intensity map has magnetic anomalies values between 43,000 nT to maximum value 43,050 nT. This map exhibits different distinct anomalous. The total magnetic map reveals a high magnetic anomaly in the northwestern part of the study area related to shallow basement relief with maximum magnetic value reaches 43,050 nT and decreasing towards the east direction. Most of the anomalies have N-S and NE-SW trends.

3.1.2. Magnetic map reduced to the pole (RTP)

In the present study, the total intensity magnetic map reduced to magnetic pole RTP which can be calculated automatically by using Geosoft Oasis Montaj (2015) using parameters such as inclination (43.3469°), declination (2.699°), field strength (49,215.7932 nT).

The inspection of the obtained RTP map (Figure 2 (b)) shows a small deviation of the spatial location of the anomalies from the original data after recalculating the data. The RTP map shows anomalies with magnitude range from 43,000 to 43,044 nT. These anomalies are classified as low and high magnetic anomalies, the low magnetic anomalies in the eastern part of the studied area which related to the deep basement relief. The northwestern part characterised by high magnetic anomaly related to the shallow basement relief. The RTP map shows that the high gradient zones are indicator of possible major fault zones; the major structural trends have the directions NE-SW and N-S (Figure 3(c)).

3.1.3. Filter of magnetic data

The filter technique of high and low pass was applied on the RTP map for isolated the regional and residual magnetic anomalies based on wavenumber. Through the

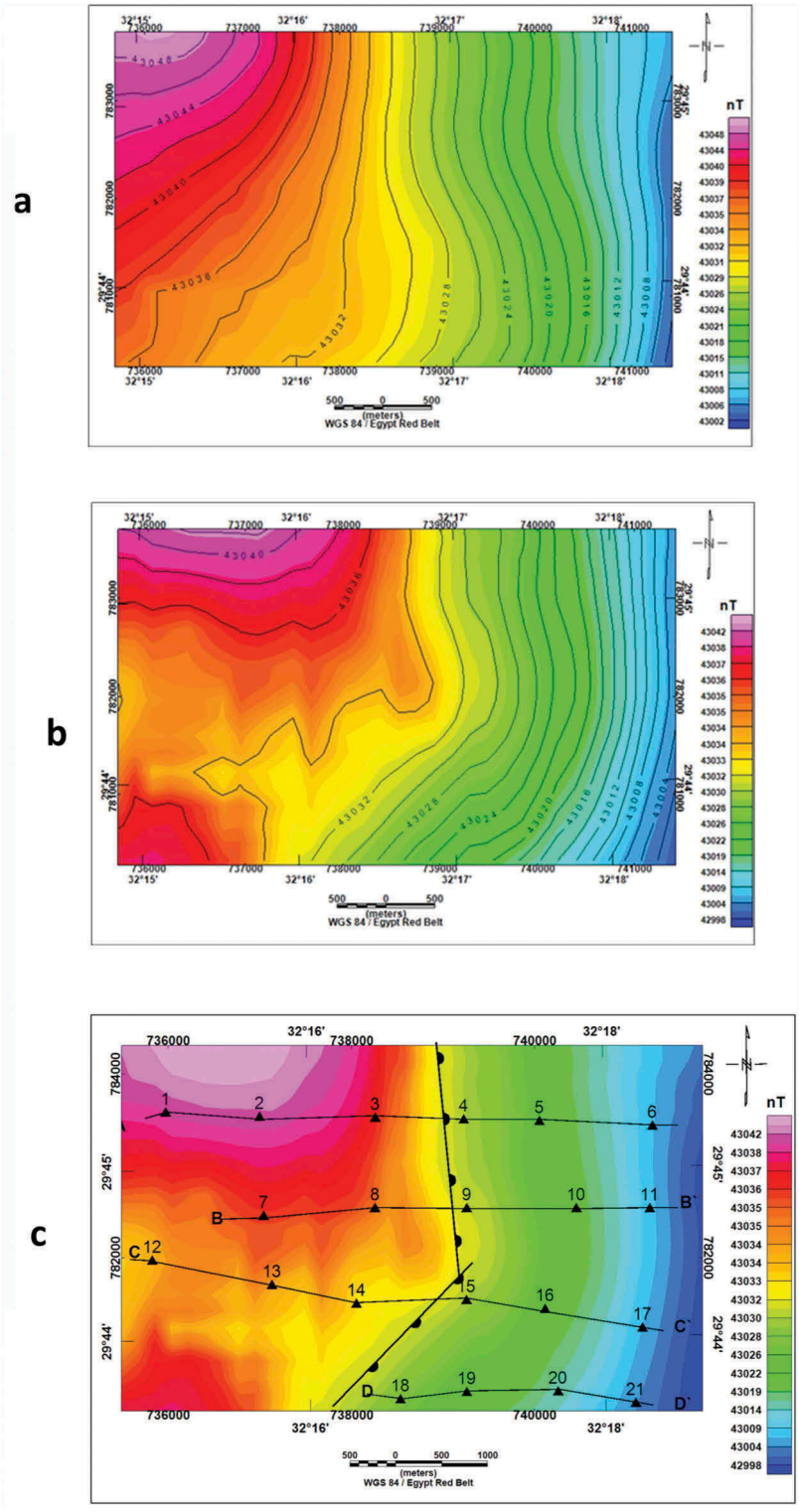

Figure 2. (a) Total Intensity Magnetic Map (TMI), (b) Total Magnetic Intensity map reduced to the north pole (RTP), (c) Fault elements dissect the study area with VES location which used for constructed geoelectric cross-section along profiles A-A`, B-B`, C-C` and D-D`.

power spectrum technique at a wave number cut-off of 0.000205 (1/km) (Figure 3(a)). The separation has been carried by using Geosoft Oasis Montaj (2015), the high pass (residual) and low pass (regional) magnetic anomaly maps represent two maps producing from RTP map. The regional anomalies of the RTP (low pass) (Figure 3(b)) reveal smoothing of the contours of the principle high and low magnetic anomalies. These maps showing that the northwestern part occupied by high magnetic anomalies and decreasing towards the eastern part of the area under study. The residual anomalies (High pass filter) (Figure 3(c)) represent a lot of local features of high and low polarities, smaller areal extensions, steeper reliefs and low amplitudes.

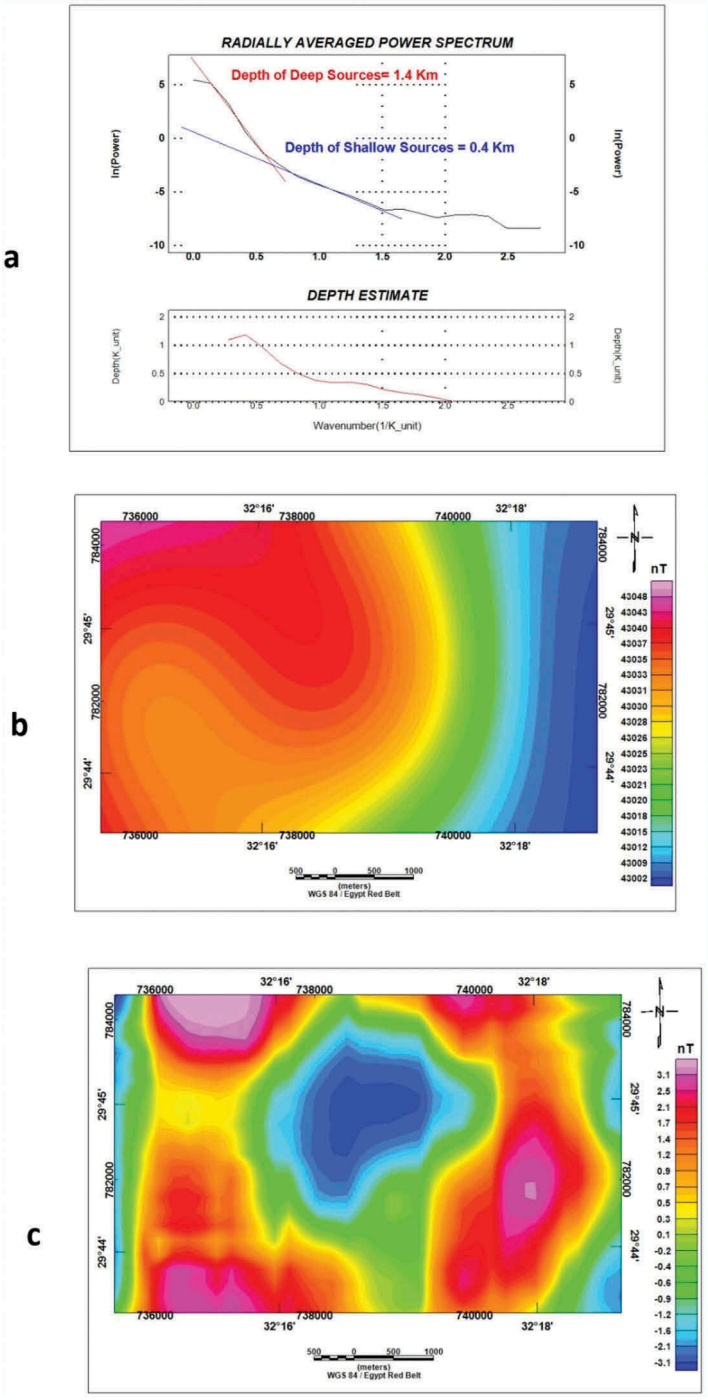

Figure 3. Magnetic separation, (a) 2-d Radially average power spectrum curve of the studied area, (b) Low Pass Filter (Regional) Map, (c) High Pass Filter (Residual) Map.

3.1.4. Upward and downward continuation

The upward and downward continuation techniques are applied on magnetic data (RTP) using Geosoft Oasis Montaj (2015) to indicates the depth of sources of deep and shallow sources. The upward continuation applied at distances 10, 500, 1000 and 2000 m, these upward maps refer to the maps are more smoothed by increasing the distance of upward where the distance 2000 m is the maximum distance of deep sources as shown in Figure 4. The downward continuation is applied at distances of 50, 100, 200 and 500 m where the distance of 500 m is the maximum distance for shallow sources as shown in Figure 4.

3.1.5. 3-D Magnetic modelling

An interpretation of the magnetic data has been carried through 3-D magnetic modelling by using the GMSYS3D software Geosoft Oasis Montaj (2015). The theoretical background and calculations are performed in the wavenumber domain Parker's algorithm Parker (1973). In this study, the conformable between

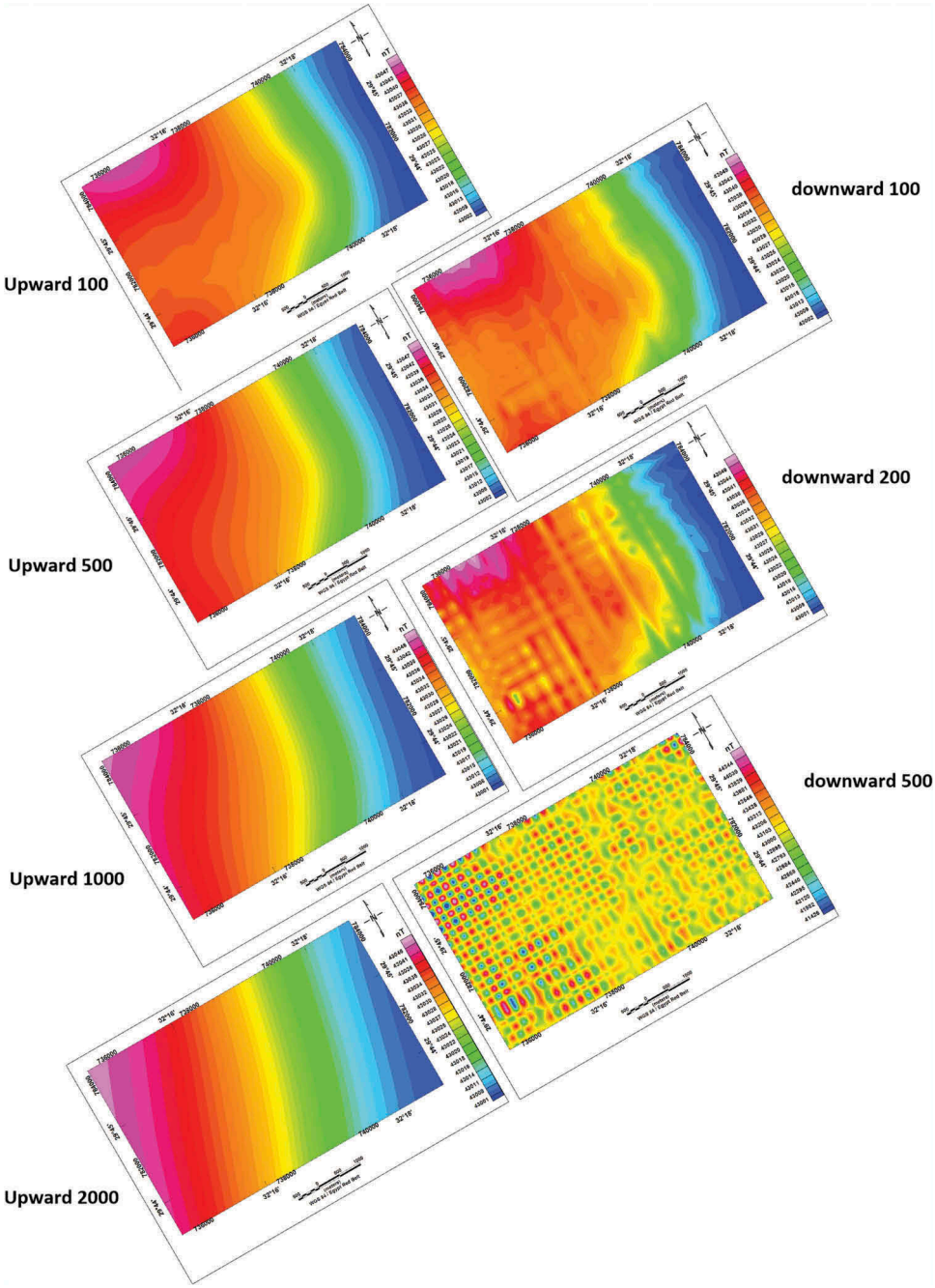

Figure 4. Upward and downward continuations at different distances.

calculated and observed maps, and percentage of error is very small (Figure 5(a–c)).

The essential benefit of the magnetic interpretation is to be used for geological mapping of the basement surface which reflects the topographic change in basement surface. For present study in groundwater exploration, the depth estimation is often used to determine the depth of basement rocks and location of geologic units and structures that produce a magnetic anomaly. From the results of 3 D modelling (Figure 6(a, b)) the depth ranges from 1998 m in the southwestern parts to 1927 m at the eastern parts of the study area.

3.2. Geoelectric data

3.2.1. Geoelectric data acquisition

The geoelectrical data consist of 21 vertical electrical soundings (VES) carried out by using Schlumberger configuration were taken at increasing current electrodes spacing (maximum half current electrode AB/2 1500 m) such that, the injected electric current should be penetrating at greater depths (ranging from 1 to 600 m depth. The VES stations were performed along four profiles (Figure 2(c)). The measurements are carried out using Sycal-R2.

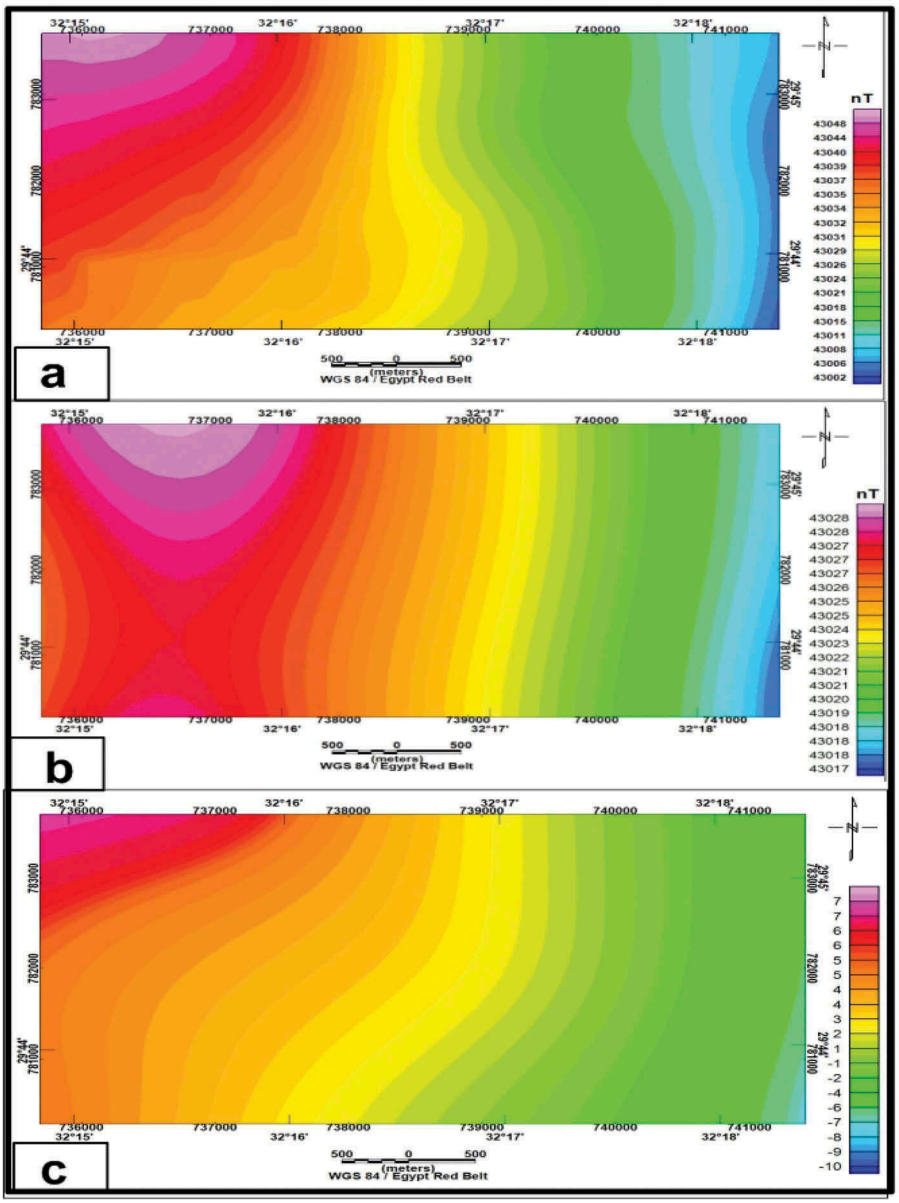

Figure 5. Outputs of GMSYS-3D modelling; (a) observed anomalies, (b) calculated anomalies and (c) deviation between calculated and measured anomalies (error).

3.2.2. Quantitative interpretation

Quantitative interpretation of the geoelectrical resistivity sounding data, the apparent resistivity values were calculated and plotted against the half spacing of electrodes (AB/2), then treated by using the IPI2WIN computer program. In this study using IPI2WIN program to determine the true resistivity and thickness by drawing theoretical and field with model curve. The results are correlated with the given well data and were used for the construction of geoelectrical cross-sections which exhibit the different geological units existing in the study area.

3.2.3. Geoelectrical cross-sections

The geoelectrical cross-sections along profiles A-A`, B-B`,C-C`and D-D` (Figure 7) indicate six geoelectric units. The first layer represents the Quaternary dry sand and gravel deposits of high resistivity from 20 Ohm.m at VES 14 to Maximum 417 Ohm.m at VES 20 and thickness ranges from 0.6 m at VES 6 to 15.5 m of largest thickness at VES 20 in the southern part of the study area. The second layer is the upper Miocene sandstone and limestone of resistivity ranges from 20 Ohm.m at VES 13 to 120 Ohm.m at VES 14 and thickness from 10 m to maximum 62 m at VES 18 this layer represents the fresh water aquifer in the study area. The third layer is the second aquifer which represents brackish water of resistivity ranges from 3 Ohm.m at VES 10 to 13 Ohm.m at VES 12 and thickness range from 11 m at VES 12 to 86 m at VES 21. The fourth layer is the lower Miocene limestone and clay limestone exhibits resistivity ranges from 18 Ohm.m at VES 3 to 90 Ohm.m at VES 12 and thickness range from 21 m at VES 12 to 107 at VES 18 m. The fifth layer is the Oligocene

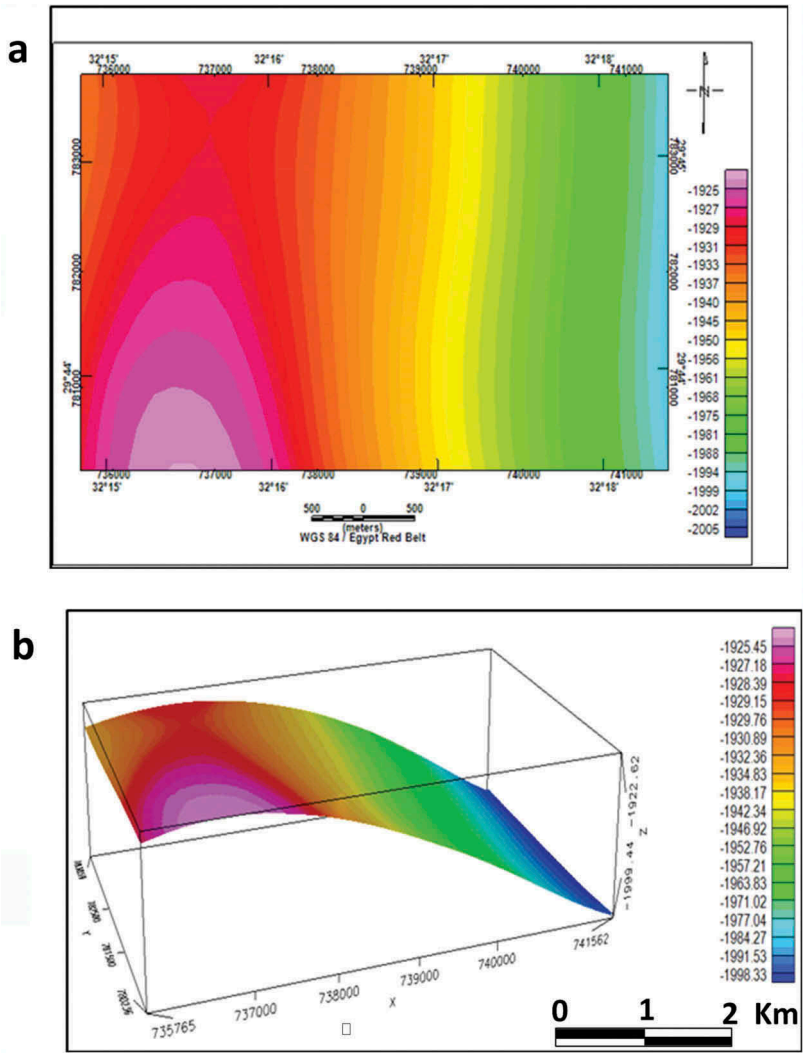

Figure 6. (a) The basement depth of the study area, (b) 3D Surface of the basement.

upper Miocene clay and sandstone exhibits resistivity ranges from 1 Ohm.m at VES 21 to 12 Ohm.m at VES 18 and thickness range from 90 at VES 12 to 134 m at VES 4. The sixth layer is the Middle Eocene limestone exhibits resistivity ranges from 19 Ohm.m at VES 19 to 97 Ohm.m at VES 3. According to the geoelectrical results and lithologic information of drilled wells, the second layer represents the major promising aquifer in the study area.

3.2.4. Isopach map of the second geoelectrical unit

The thickness of the second layer ranges from 10 m to maximum 64 m at VES 18. The isopach map of this unit showing high thickness in the southern part of the study area while the western part is characterised by low thickness (Figure 8(a)).

3.2.5. Depth map of the second geoelectrical unit

The depth map for the top surface of the aquifer (Figure 8(b)) indicates that the southern part is deeper while the depth is shallower towards northwestern, northeastern and southeastern regions of the study area.

3.2.6. Isoresistivity map of the second geoelectrical unit

The resistivity values range from 20 Ohm.m at VES 13 to 120 Ohm.m at VES 14. The resistivity increasing in the middle of the southern part of the study area (Figure 8(c)).

3.2.7. Priority map

Figure 8(d) represents priority map for drilling plan in the future for the study area where zone (A) represents the best locations for drilling. The zone (A) indicates high thickness, low depth and high resistivity values for the fresh water aquifer, then zone (B) which represents high thickness and high resistivity values while zone (C) represents low thickness, low depth and high resistivity values.

4. Discussion

The results of integrated geological and geophysical data are conformed to each other where the fault elements which dissect the study area and coming from the interpretation of magnetic data are

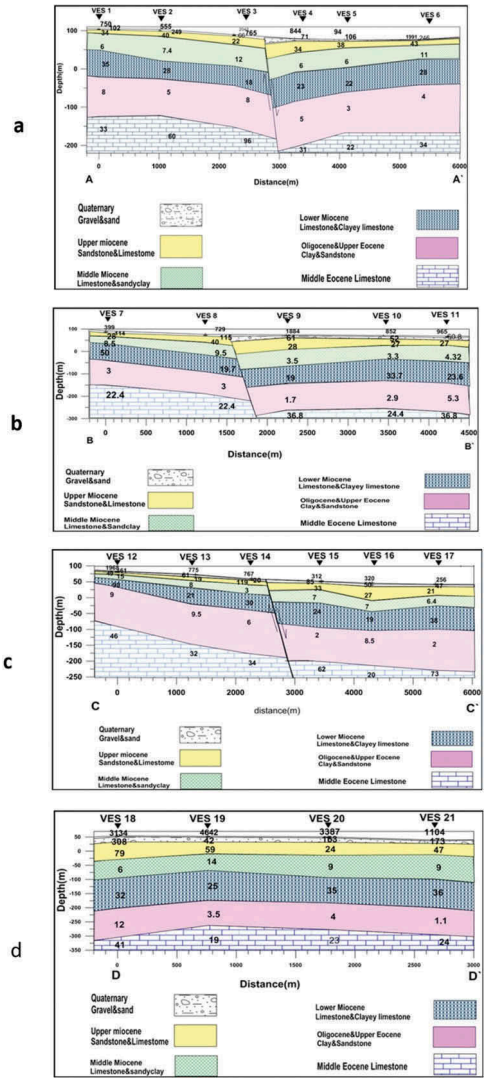

Figure 7. Geoelectrical cross sections along profiles A-A`, B-B`, C-C` and D-D`.

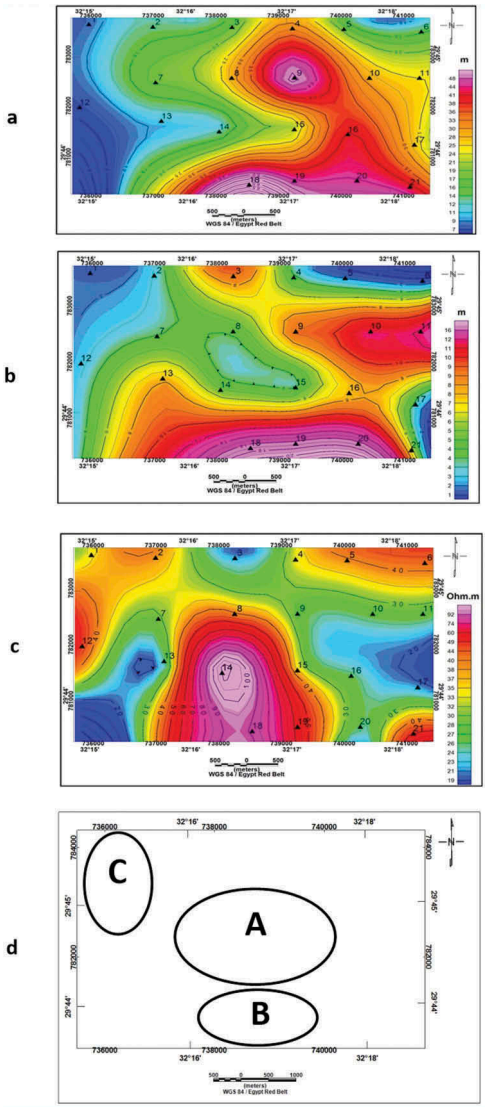

Figure 8. (a) Isopach map of the second geoelectrical unit, (b) Depth map of the second geoelectrical unit, (c) Isoresistivity map of the second geoelectrical unit, (d) Priority map for future drilling plan.

conformed by results of geoelectrical data. The depth of basement rocks from the 3-D magnetic modelling is conformed by the power spectrum analysis of magnetic data. The results of geoelectric data indicate that the study area include two aquifers, the first aquifer is the fresh water aquifer and the second is the brackish water aquifer these results are conformed with results of boreholes which drilled around the study area.

5. Conclusion

Based on the interpretation results, it can be concluded that: The depth to the basement surfaces ranges from 1927 to 1998 m and the main trends of structural elements have directions N-S and NE-SW trends. The area under study is formed mainly of six different geoelectrical layers. These layers related to the Quaternary sediments, Upper Miocene sediments, Middle Miocene sediments, Lower Miocene sediments, Oligocene and Upper Eocene sediments and Middle Eocene sediments. The groundwater is accumulated in two aquifers: the first is the Upper Miocene represents the fresh water aquifer while Middle Miocene, deposits represent the brackish water aquifers. The depth to surface of fresh water aquifer varies from 1 m in the northern part to 17 m in the southern part and thickness varies from 10 m to 64 m in the southern part of the investigated area. The central part of the study area represents the best location for future drilling plan.

Disclosure statement

No potential conflict of interest was reported by the authors.

ORCID

Sultan Awad Sultan Araffa http://orcid.org/0000-0002-7098-918X

References

Abdallah AM, Adindani A, Fahmy N. 1963. Stratigraphy of the lower Mesozoic rocks, western side of the Gulf of Suez. Geol. Surv. and Min. Res Depart. Egypt, Paper No. 27; p. 23.

Abdel Khalek ASM. 2014. Structural modeling of Wadi Ghoweiba segment, the Northwestern Sector of the Gulf of Suez Rift [Egypt. MSc]. Geology Department Faculty of Science Cairo University; p. 163.

Abdellatif Y, Osman MO, Amin EK, Mohd N, Mamdouh S, Elhamy AT. 2019. Assessment groundwater occurrences using VES/TEM techniques at North Galala plateau, NW Gulf of Suez, Egypt. J Afr Earth Sci. 160(2019):103613. doi:10.1016/j.jafrearsci.2019.103613.

Araffa SAS, Mohamed AME, Santos FM. 2017. Geophysical investigation in the Northwestern part of the Gulf of Suez, Egypt. Egypt J Pet. 1:19.

Araffa SAS, Mousa SEA, Salama OHM, Mesbah HS. 2014. Joint inversion of resistivity (VES) and time domain electromagnetic (TEM) data for groundwater exploration at wadi hagul, northeastern part of eastern desert, Egypt. Egs J. 12(1):29–40.

Awad GH, Abdallah AM. 1966. Upper Cretaceous, Eastern Desert, with emphasis on neighboring areas. J Geol. 10 (2):125–144.

Ball J. 1900. On the origin of the Nile valley and Gulf of Suez. Cairo Sci J III. 37:250–252.

Conoco C. 1987. Geological map of Egypt, scale 1: 500,000-NF 36 NE-Bernice, Egypt. Cairo: The Egyptian General Petroleum Corporation.

Desouki HA, Gomaa MA, Sadek MA, Ezz El –Deen HA. 2006. Hydrochemical and isotopic evaluation of groundwater quality, El Ain El—Sukhna and Wadi Araba localities, aquifers, Egypt. Mansoura J Geol Geophy. 33(1):32–64.

El Osta MM, El Sheikh A, Barseem MS. 2010. Comparative hydrological and geoelectrical study on the Quaternary aquifer in the deltas of Wadi Badaa and Ghweiba, El Ain El Sukhna area, Northwest Suez Gulf, Egypt. Int J Geophy. 2010:15. Article ID 585243. doi:10.1155/2010/585243.

El Shazly EM. 1977. The Geology of the Egyptian Region. New York: Plenum Press. A. E. M. Nairn et al. Chapter 8; p. 379, 444.

Farag IAM, Ismail MM. 1959. A contribution to the structure of the area east of Helwan, Egypt. Egypt J Geol. 3 (I):71–86.

Farhoud K. 2009. Accommodation zones and tectono-stratigraphy of the Gulf of Suez, Egypt: a contribution from aeromagnetic analysis. GeoArabia. 14(4):139–162.

Geosoft Oasis Montaj, 2015. Data processing and analysis systems for earth science applications (Ver. 8.3.3). Geosoft Inc, Toronto, Canada. Accessed 2015. www.geosoft.com.

Ghorab MA. 1961. Abnormal stratigraphic features in Ras Gharib oil field. The 3rd Arab Petrol. Congr; Alexandria, Egypt. p. 10.

Hassan SM. 2008. Studying of geological structures of Ayn-Sokhna area, north Eastern Desert Egypt, by optimum utilization of data fusion techniques of some satellite image [Ph.D. Thesis]. Faculty of science, Helwan University; p. 207.

Hewaidy AA, El-Motaal EA, Sultan AS, Talaat MR, Ahmed AE, Shokry AS. 2015. Groundwater exploration using resistivity and magnetic data at the northwestern part of the Gulf of Suez, Egypt. Egypt J Pet. 24:255–263. doi:10.1016/j.ejpe.2015.07.010.

Parker RL. 1973. The rapid calculation of potential anomalies. Geophys J Int. 31(4):447–455. doi:10.1111/j.1365-246X.1973.tb06513.x.

Sadek H. 1926. The geography and geology of the district between Gebel Ataqa and El Galala El-Bahariya, Gulf of Suez. Geol Surv Egypt. 9:120.

Said R. 1962. The geology of Egypt. Amsterdam: Elsevier Pub. Co.; p. 377.

Strougo A. 1986. The velascoensrs event: A significant episodes of tectonic activity in the Egyptian Paleogene. Neues Jahrb Geol Palaontol Abh. 173:253–269.

Sultan AS, Essa KSAT, Khalil MH, El-Nahry AEH, Galal ANH. 2017. Evaluation of groundwater potentiality survey in south Ataqa-northwestern part of Gulf of Suez by using resistivity data and site-selection modeling. NRIAG J Astron Geophys. 6(1):230–243. doi:10.1016/j.nrjag.2017.02.002.